Molecular Crystals and Liquid Crystals

ISSN: 1542-1406 (Print) 1563-5287 (Online) Journal homepage: http://www.tandfonline.com/loi/gmcl20

Liquid Crystal Control of Surface Plasmon Resonance Sensor Based on Nanorods

Victor Yu. Reshetnyak, Igor P. Pinkevych, Victor I. Zadorozhnii & Dean R. Evans

To cite this article: Victor Yu. Reshetnyak, Igor P. Pinkevych, Victor I. Zadorozhnii & Dean R. Evans (2015) Liquid Crystal Control of Surface Plasmon Resonance Sensor Based on Nanorods, Molecular Crystals and Liquid Crystals, 613:1, 110-120, DOI: 10.1080/15421406.2015.1032080

To link to this article: http://dx.doi.org/10.1080/15421406.2015.1032080

Mol. Cryst. Liq. Cryst., Vol. 613: pp. 110–120, 2015

ISSN: 1542-1406 print/1563-5287 online
DOI: 10.1080/15421406.2015.1032080

Liquid Crystal Control of Surface Plasmon Resonance Sensor Based on Nanorods

VICTOR YU. RESHETNYAK,[1] IGOR P. PINKEVYCH,[1]
VICTOR I. ZADOROZHNII,[1,*] AND DEAN R. EVANS[2]

[1]Taras Shevchenko National University of Kyiv, Physics Faculty, Kyiv, Ukraine
[2]Air Force Research Laboratory, Materials and Manufacturing Directorate, Wright-Patterson Air Force Base, Ohio, USA

We analyze a theoretical model of the five layer nanorod-mediated surface plasmon resonance (SPR) sensor comprising a nematic LC layer. The light propagation through the layered system is studied solving the Fresnel equations under SPR conditions. We calculate the light reflectance angular spectrum and show that control of the orientational state of the LC layer enables us to manipulate position of the reflectance curve minimums, their depth and sensitivity. It allows one to choose an interval of the light incidence angles convenient for work without need in angular tuning of sensor at replacing of the analyte.

Keywords surface plasmons; liquid crystal; columnar thin film; sensing

1. Introduction

Resonant coupling of photons from p-polarized incident light to free electron oscillations in noble metals and the resulting excitation of surface plasmons (SP) under the surface plasmon resonance (SPR) conditions has been widely employed in sensor applications for monitoring chemical and biochemical binding events on surface. In the SPR sensing technique the reflected beam strength is measured for different incidence angles and a dip in the reflectivity is observed at a certain angle. This angle is very sensitive to the refractive index of the layer adjacent to the layer where SP arises [1]. In recent years, different modified SPR sensing systems were proposed [2]. Many works were done on optimizing SPR sensor characteristics: modifying prism refractive index, optimizing metallic layer, and using bi-metallic layer [3–7]. The performance of the SPR sensing technique was also analyzed for light beams with finite cross-sections [8]. In paper [9] the nanorod-mediated SPR sensor was investigated in which localized surface plasmons (LSP) were generated in an additional anisotropic layer of aligned silver nanorod array. SPR properties of such a sensor were enhanced due to interaction between SPs and LSPs.

In the present paper the nanorod-mediated SPR sensor which comprises an additional layer of nematic liquid crystal (LC) will be considered. We shall study how controlling the orientatation state of the LC layer allows one to manipulate the features of the sensor.

*Address correspondence to V. I. Zadorozhnii, Taras Shevchenko National University of Kyiv, Physics Faculty, 64/13, Volodymyrska Str., Kyiv, 01601, Ukraine. E-mail: viza@univ.kiev.ua

The paper is organized as follows. In Section 2 we describe the SPR sensor scheme with the LC layer. In Section 3 we present dielectric functions of the media composing the layers. In Section 3 we introduce equations to be solved. Results of calculations and discussion are presented in Section 4. Finally, in Section 5 we present the brief conclusions. The cumbersome reflection and transmission coefficients are outlined in the Appendix.

2. Scheme of the Five-Layer SPR Sensor

Let us consider the five-layer model of a SPR sensor in the extended-range geometry [10] (Fig.1). A monochromatic p-polarized light is incident in the x-z plane on the plane interface between the cylindrical glass prism 1 and the LC layer 2 with thickness h_{LC}. Layer 3 is a thin metal film (Ag in our study) of thickness d_f with complex permittivity ε_3. Next is layer 4, which is an aligned nanorod array with thickness d_e, comprised of inclined metallic (Ag) nanorods lying in the xz-plane with voids between them. The material of the target analyte (sensing layer 5) and voids between nanorods are the same.

With an increase of the incidence angle θ, at a certain value $\theta = \theta_{SPR}$ in the region of total internal reflection of the glass prism, the momentum of the incident light transferred by the evanescent wave through the LC-layer perfectly matches the SPs momentum at the interface of layers 3 and 4. Under these conditions the SP resonance (SPR) occurs. It results in the appearance of a minimum in the reflected light intensity at the angle θ_{SPR}. Interaction between SPs and LSPs arising in the nanorods (Layer 4) influences SPR, in particular, it shifts the position of minimum in SPR curve [11,12]. Nanorods surface also provides more reaction area for the target analyte that enhances sensitivity of the sensor [13,14,9].

The LC layer acts here as a several light wavelength thick tunnel barrier to excite SPs on the bottom surface of the metal layer [15]. Besides, in the LC layer the half-leak modes can propagate [16]. Properties of the LC depend on its orientational state. Changing the orientational state of the LC layer by external (e.g. magnetic) field allows the manipulation of the features of the SPR curve.

3. Dielectric Functions of the Media Constituting Layers

Nematic LC (layer 2) is a uniaxial medium whose dielectric function at optical frequencies can be written as $\varepsilon_{LC\,ij} = n_o^2\delta_{ij} + (n_e^2 - n_o^2)d_i d_j$, where d_i is the director Cartesian compo-

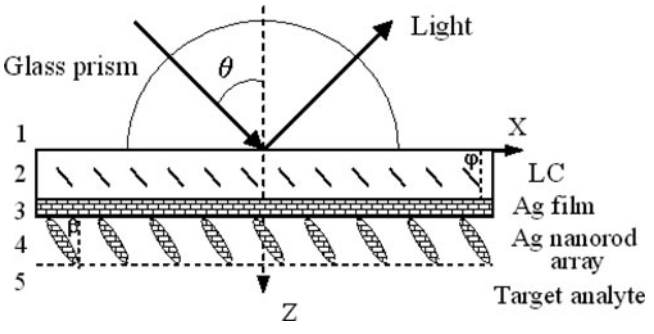

Figure 1. Schematic of the 5-layer nanorod-mediated SPR sensor.

nent, n_o and $n_e$are the ordinary and extraordinary refractive indices, respectively, $\delta_{ij}$is the Kronecker symbol. We shall neglect the small absorption in the LC layer.

Let the director lie in the x-z plane and be subject to a very weak anchoring at the LC layer substrates. We also suppose that the incident light wave intensity is small and does not disturb the director. Then, denoting the angle of the director with the z-axis by φ and parameterizing the director as follows, $d = \{\sin\varphi, 0, \cos\varphi\}$, we put, for simplicity, the angle φ to be constant over the LC layer.

For p-polarized incident wave ($E_y = H_x = H_z = 0$) the wave inside the LC layer is the extraordinary one. Its wave vector depends on the incidence angle θ and has different values for waves traveling in the forward direction and the reversed direction after reflection [17,18]. In particular, the z-projection of the wave vector of these waves follows from Maxwell's equations and has the form [17]:

$$k_{2z\pm} = k_0 \frac{-n_1 \sin\theta\, \varepsilon_{LC\,xz} \pm n_o n_e \sqrt{\varepsilon_{LC\,zz} - n_1^2 \sin^2\theta}}{\varepsilon_{LC\,zz}}, \tag{1}$$

where the plus (minus) sign corresponds to the wave propagating in the forward (backward) direction, n_1 is the refractive index of the glass prism, $k_0 = \omega/c$, $\varepsilon_{LC\,zz} = n_o^2 \sin^2\varphi + n_e^2 \cos^2\varphi$ and $\varepsilon_{LC\,xz} = (n_e^2 - n_o^2)\ \sin\varphi\ \cos\varphi$. Note, that the component of the incident wave vector $k_x = k_0\, n_1 \sin\theta$ remains constant in each interface of the sensor, so that $k_{2x\pm} = k_x$.

The LC dielectric function $\varepsilon_{2\pm}$ for these waves can be then obtained from equation $\varepsilon_{2\pm} = (k_x^2 + k_{2z\pm}^2)/k_0^2$ and reads as (see also [19])

$$\varepsilon_{2\pm} = n_1^2 \sin^2\theta + \left[\frac{-n_1 \sin\theta\, \varepsilon_{LC\,xz} \pm n_o n_e \sqrt{\varepsilon_{LC\,zz} - n_1^2 \sin^2\theta}}{\varepsilon_{LC\,zz}} \right]^2. \tag{2}$$

We adopt the one-pole Drude-Lorentz-Sommerfeld formula for the dielectric function of the thin metallic layer (layer 3) and metallic nanorods in layer 4, which is reasonably accurate in the wavelength range of interest for sensor applications [20–22]:

$$\varepsilon(\omega) = 1 - \frac{\omega_p^2}{\omega\ [\omega + i\,\alpha\,\gamma(L_{eff})]} + \frac{\tilde{f}\,\omega_b^2}{\omega_b^2 - \omega^2 - i\,\zeta\,\omega\,\Gamma_b}, \tag{3}$$

where the last term in (3) is the contribution of the bound valence electrons of the ion cores, ω_p is a plasma frequency, $\tilde{f}$ is a weighting factor (oscillator strength), ω_b and Γ_b are the bound-electron resonant frequency and decay constant, respectively, α and ζ are adjustable parameters, $\gamma(L_{eff})$ is a damping constant of the free electron motion dependent on effective mean free path of electrons, L_{eff}. In the nanorods $\gamma(L_{eff})$ is given by [23]

$$\gamma(L_{eff}) = \gamma_\infty + \gamma_{surf} = \gamma_\infty + A\, v_F / L_{eff}, \tag{4}$$

where γ_∞ is the scattering rate of the free electrons in the bulk metal, v_F is velocity of electrons on the Fermi surface, A is a parameter of order unity, depending on the features of the particle surface scattering. The term γ_{surf} accounts for the additional damping due to the increase in slightly inelastic scattering of free electrons at the particle surface when the size of the particle is smaller than the electron free path [23,24].

We use a geometrical probability model for calculating L_{eff} in nanorods of spheroidal shape [25]. In this model L_{eff} is expressed in terms of geometrical invariants and takes

the form $L_{eff} = 4V/S$, where V is the nanorod volume and S is its surface area. Explicit expressions for L_{eff} are presented in paper [9].

Nanorod array represents the oblique columnar microstructure with tilting angle β in the plane parallel to the x-z plane (Fig.1). Optical properties of this anisotropic layer are described by dielectric constant tensor ε_4 [26]

$$\varepsilon_4 = \begin{pmatrix} \varepsilon_{x'} \cos^2\beta + \varepsilon_{z'} \sin^2\beta & 0 & (\varepsilon_{z'} - \varepsilon_{x'}) \sin\beta \cos\beta \\ 0 & \varepsilon_{y'} & 0 \\ (\varepsilon_{z'} - \varepsilon_{x'}) \sin\beta \cos\beta & 0 & \varepsilon_{x'} \sin^2\beta + \varepsilon_{z'} \cos^2\beta \end{pmatrix}, \tag{5}$$

where $\varepsilon_{x\prime} = \varepsilon_{y\prime}$,$\varepsilon_{z\prime}$ are effective dielectric constants in the coordinate system of spheroids and can be calculated using the effective medium theory [27,28]. Considering the analyte embedded in an aligned metal nanorod array (in array voids) as the host and using the Maxwell-Garnett theory to calculate the effective dielectric tensor of the anisotropic layer 4 we obtain that [27,28]

$$\varepsilon_j = \varepsilon_3 \left[1 + (1 - f_m) \frac{\varepsilon_5 - \varepsilon_3}{f_m L_j (\varepsilon_5 - \varepsilon_3) + \varepsilon_3} \right], \tag{6}$$

where $j = x'$, y', z', f_m is the volume fraction of metal (Ag), ε_3 is the dielectric constants of metal (i.e. formula (3) for metal nanorods) and ε_5 is the dielectric constant of the analyte, L_j is the depolarization factor calculated and presented in paper [29].

Similarly to eqs. (1)–(2) for anisotropic layer 2 we can also obtain the wave vector for the z-projection and the dielectric function of the waves propagating in the forward and backward directions in anisotropic layer 4

$$k_{4z\pm} = k_0 \frac{-n_1 \sin\theta\, \varepsilon_{4xz} \mp \sqrt{\varepsilon_{z'} \varepsilon_{x'} \left(\varepsilon_{4zz} - n_1^2 \sin^2\theta \right)}}{\varepsilon_{4zz}}, \tag{7}$$

$$\varepsilon_{4\pm} = n_1^2 \sin^2\theta + \left[\frac{-n_1 \sin\theta\, \varepsilon_{4xz} \mp \sqrt{\varepsilon_{z'} \varepsilon_{x'} \left(\varepsilon_{4zz} - n_1^2 \sin^2\theta \right)}}{\varepsilon_{4zz}} \right]^2. \tag{8}$$

Thickness of the nanorod-array layer can be calculated using the shape and size of the nanorods.

4. Calculation Scheme

In order to investigate the SPR sensor properties associated with adding of the LC layer, we use the 5-layer model of the sensor and study the propagation of p-polarized incident light through the layered system shown in Fig. 1. In our model we deal with a system of alternating isotropic (1, 3, 5) and anisotropic (2, 4) layers, each of which is characterized by the corresponding dielectric function. The relevant computational scheme for calculation of light propagation in the 5-layer system is presented in

We take in account the phenomenon of nonsymmetrical reflection at the boundaries between anisotropic and isotropic layers [26, 27]. Then, using the approach described in [30, 31], we obtain the following system of equations for propagation of p-polarized waves

in the 5-layer system:

$$R_1 - t_{21}A_{2-} = r_{12}, \tag{9}$$

$$A_{2+} - r_{21}A_{2-} = t_{12}, \tag{10}$$

$$A_{2-}\exp(i\,k_{2z-}h_{LC}) - r_{23}A_{2+}\exp(i\,k_{2z+}h_{LC}) - t_{32}A_3 = 0, \tag{11}$$

$$t_{23}A_{2+}\exp(i\,k_{2z+}h_{LC}) + r_{32}A_3 - T_3 = 0, \tag{12}$$

$$A_3\exp(i\,k_{3z-}d_f) - r_{34}T_3\exp(i\,k_{3z+}d_f) - t_{43}A_{4-} = 0, \tag{13}$$

$$r_{43}A_{4-} + t_{34}T_3\exp(i\,k_{3z+}d_f) - A_{4+} = 0, \tag{14}$$

$$r_{45}A_{4+}\exp(i\,k_{4z+}d_e) - A_{4-}\exp(i\,k_{4z-}d_e) = 0, \tag{15}$$

$$t_{45}A_{4+}\exp(i\,k_{4z+}d_e) - T_5 = 0 \tag{16}$$

where $k_{jz} = \sqrt{\varepsilon_j k_0^2 - k_x^2}$ $(j = 1 \ldots 5)$, $k_x = \sqrt{\varepsilon_1}k_0 \sin\theta$; r_{ij} and t_{ij} are reflection and transmission coefficients at the boundary of the i-th and j-th layers [30], R_1 and T_5 are the reflection and transmission coefficients of the hybrid sandwiched film, A_j $(j = 2, 3, 4)$ and T_3 are the ratios of the magnetic field magnitude at the beginning of the j-th layer to the incident magnetic field magnitude in the layer 1 (see. Fig.2). The sign "+" or "-" in the subscript of $k_{jz\pm}$ denote the sign of the projection of the wave vector onto the z-axis and also notes the corresponding amplitude $A_{j\pm}$.

Solving the system of equations (9)–(16) we can calculate the reflectance R of the 5-layer system defined as

$$R = |R_1|^2 . \tag{17}$$

Expressions for coefficients r_{ij} and t_{ij} at each interface appearing in (9)–(17) are given in Appendix.

5. Results and Discussion

For numerical calculation we use the following parameters. Thicknesses of layers in our model are $h_{LC} = 2.5$ μm for LC, $d_f = 40$ nm for metal (Ag) layer and $d_e = 28.8$ nm for nanorods of diameter $D = 30$ nm and length $l = 10$ nm, volume fraction $f = 0.4$ and tilting angle of the oblique columnar microstructure $\beta = 73^\circ$ [9]. The wavelength of incident light is $\lambda = 632.8$ nm; the refractive index of a glass prism is $n_1 = 1.51$.

The reflectance in Fig. 3 is calculated for experimentally often used nematic LCs having different refractive indices and birefringence: 5CB ($n_e = 1.7060, n_o = 1.5319, \Delta n = 0.1741$), E7 ($n_e = 1.7303, n_o = 1.5189$, $\Delta n = 0.2114$), and E44 ($n_e = 1.7753$, $n_o = 1.5240, \Delta n = 0.2513$) [32]. The dielectric function (3) of the metal (Ag) layer calculated for $\lambda = 632.8$nm using data of paper is $\varepsilon_3 \approx -18.3714 + i0.4710$ [22].

Using numerical data mentioned above we calculated the reflectance $R$of the 5-layer system as function of the light incident angle θ for different director orientation in the LC layer (Fig. 3). It is seen that the curve $R(\theta)$has several minimums, which arise due to mixing of the extended-range-type SP mode with the half-leak modes propagating in the LC layer

if the incidence angle θ falls in the range [16]

$$\arcsin\sqrt{\frac{\mathrm{Re}(\varepsilon_3)}{\varepsilon_1}} < \theta < \arcsin\sqrt{\frac{n_o^2 + \left(n_e^2 - n_o^2\right)\cos^2\varphi}{\varepsilon_1}}. \tag{18}$$

We can also see that the angular spectrum (position and depth of minimums) of the reflected light depends strongly on the director orientation in the LC layer. Besides, it is seen the nonmonotonic dependence of the reflectance minimum position on the LC birefringence. A qualitative picture of the angular spectrum $R(\theta)$observed in Fig. 3 takes also place for nanorods with length 30 and 60 nm.

In Fig. 4 there is shown influence of the analyte refractive index on the angular spectrum$R(\theta)$ of the 5-layer sensor. Calculations were done, as an example, for the case of the LC layer filled by the LC E7 with director orientation angle $\varphi = 20^\circ$.

As we can see from Fig. 4 in the 5-layer scheme of sensor unlike the 4-layer scheme without the LC layer [9] the analyte refractive index influences the depth and width of

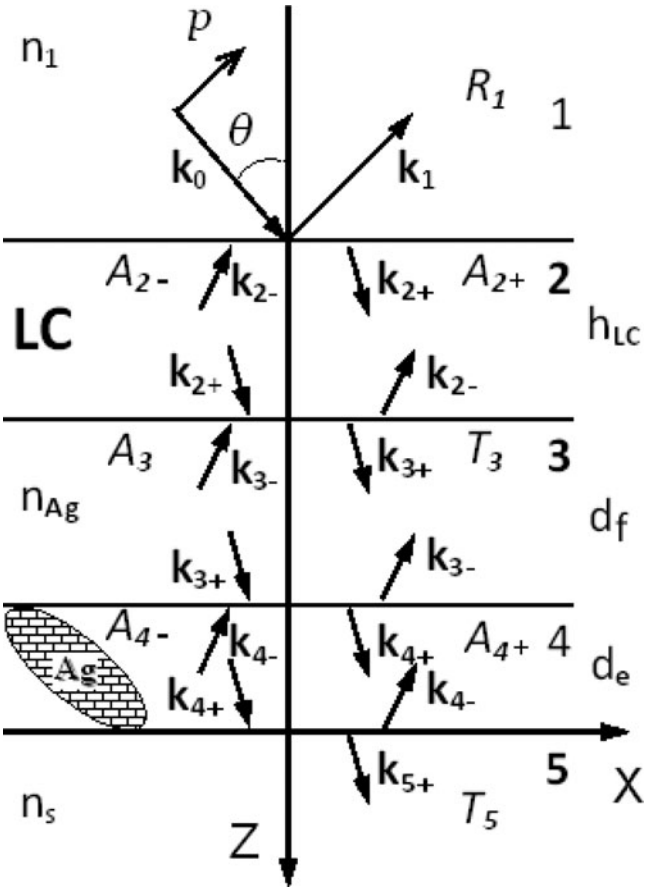

Figure 2. Computation scheme for calculation of light propagation in the 5-layer sensor system. $A_{i\pm}$, T_i, R_1 are amplitudes of waves, h_{LC}, d_f, d_e are thicknesses of layers, n_1, n_{Ag}, n_s are refractive indices.

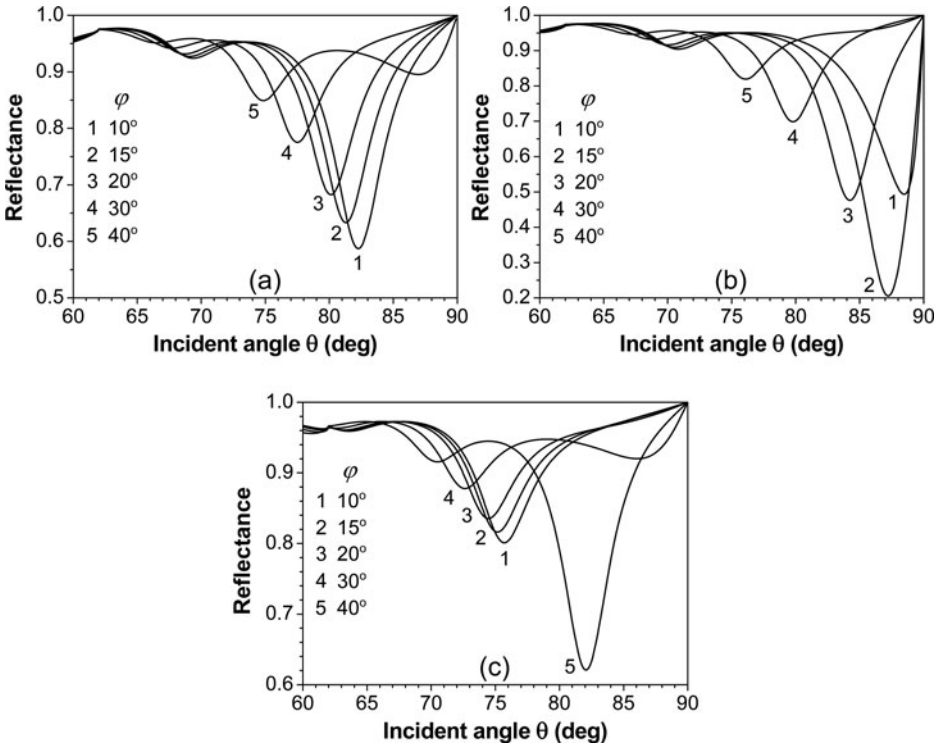

Figure 3. Reflectance R versus the light incidence angle θ for a sequence of the nematic director angles φ in the LC layer: 5CB (a), E7 (b), and E44 (c). $\varphi = 10^\circ$- 1, 15°- 2, 20°- 3, 30°- 4, 40°- 5. The analyte refractive index $n_s = 1.333$.

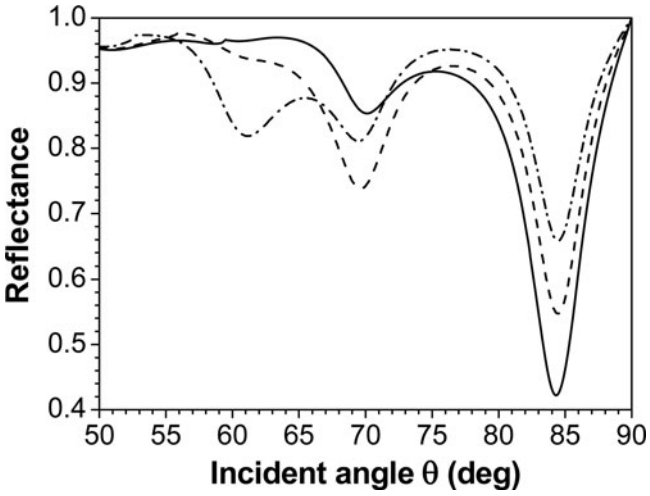

Figure 4. Reflectance R versus the light incidence angle θ for a sequence of the refractive indices n_s of the target analyte: $n_s = 1.3$- solid line, 1.25- dashed, 1.2- dot-dashed. The director orientation angle in the layer of LC E7 equals $\varphi = 20^\circ$.

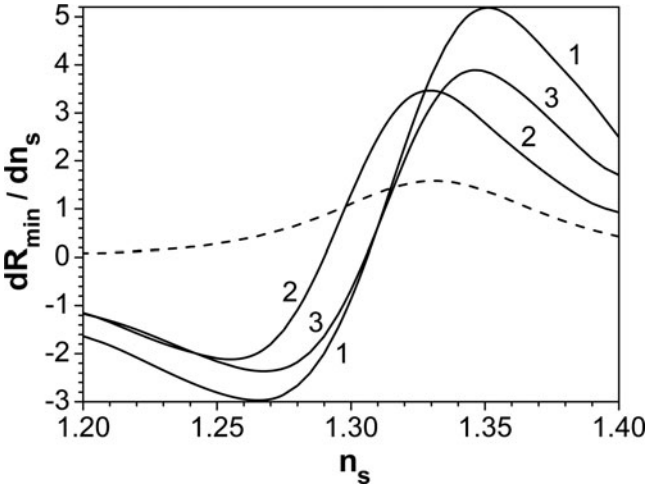

Figure 5. The effect of nematic director angle φ on the reflectance minimum sensitivity to the analyte refractive index: $\varphi = 20^\circ$- 1, $\varphi = 35^\circ$- 2, $\varphi = 50^\circ$- 3. LC layer is filled with LC E7. The dashed line shows the sensitivity in the 4-layer model of the SPR sensor of Fu et al. [9].

the reflectance minimums and practically does not influences position of minimums. We speculate that weak influence of the analyte on the reflectance minimums position is conditioned by interaction of the extended-range-type SP mode with the half-leak modes propagating in the LC layer since a condition of their arising (18) does not depend on the analyte refractive index. This can be an advantage of the 5-layer scheme because there is no need in angular tuning of sensor at replacing of the analyte. Note that any of the reflectance minimums can be chosen for analysis depending on the incidence angle interval used.

We note that in the scheme presented in this study (fixed angle of a nematic director orientation) the analyte refractive index influences mainly the depth of the reflectance minimums. Thus, the sensitivity of the proposed sensor can be characterized by change of the SPR minimum depth with the analyte refractive index change, $dR_{\min}/dn_s$.

In Fig. 5 the sensitivity of the deepest reflectance minimum to the analyte refractive index in the 5-layer scheme is shown at different director angles. Here it is also presented the corresponding sensitivity of the 4-layer (without LC) scheme of the sensor. One can see that the sensitivity of the 5-layer sensor increases with increase of the analyte refractive index depending on the director orientation angle and can appreciably exceeds the sensitivity of the 4-layer sensor. Besides, as calculations show the deepest reflectance minimum in the 5-layer scheme is much narrow than in the 4-layer scheme: ratio of half-widths of the corresponding dips in the reflectance curves, Δ_{5l}/Δ_{4l}, approximately equals one-third.

6. Conclusions

We studied a theoretical model of the 5-layer nanorod-mediated SPR sensor comprising a nematic LC layer. We show that angular spectrum of the light reflectance has several minimums arising due to mixing of the extended-range-type SP mode with the half-leak modes and depends on the LC layer orientational state. The results suggest that control of the orientational state of the LC layer enables us to manipulate the position of the reflectance curve minimums, their depth and sensitivity. It allows one to choose an interval of the light

incidence angles convenient to use. Since the analyte refractive index practically does not influence the reflectance minimum position there is no need in angular tuning of sensor at replacing of the analyte. Our results may be used for designing a new type of SPR sensor.

Funding

The work was partially supported by the EOARD Grant 118007.

References

[1] Homola, J. (2008). *Chem. Rev.*, *108*, 462.
[2] Shalabney, A., & Abdulhalim, I. (2011). *Laser & Photonics Reviews*, *5*, 571.
[3] Jha, R., & Sharma, A. K. (2009). *Opt. Lett.*, *34*, 749.
[4] Herminjard, S., Sirigu, L., Herzig, H. P., Studemann, E., Crottini, A., Pellaux, J-P., Gresch, T., Fischer, M., & Faist, J. (2009). *Optics Express*, *17*, 293.
[5] Roh, S., Chung, T., & Lee, B. (2011). *Sensors*, *11*, 1565.
[6] Kasztelanic, R. (2011). *Opt. Applicata*, *41*, 145.
[7] Perdiguero, J. M., Retolaza, A., Otaduy, D., Juarros, A., & Merino, S. (2013). *Sensors*, *13*, 13960.
[8] Anous, N. H., & Khalil, D. A. (2014). *Appl. Optics*, *53*, 2515.
[9] Fu, J., Park, B., & Zhao, Y. (2009). *Appl. Opt.*, *48*, 4637.
[10] Kou, E. F. Y., & Tamir, T. (1988). *Appl. Opt.*, *27*, 4098.
[11] Mock, J. J., Hill, R.T., Tsai, Yu-Ju, Chilkoti, A., & Smith, D.R. (2012). *Nano Lett.*, *12*, 1757.
[12] Byun, K. M., Jang, S. M., Kim, S. J., & Kim, D. (2009). *J. Opt. Soc. Am. A*, *26*, 1027.
[13] Byun, K. M., Yoon, S. J., Kim, D., & Kim, S. J. (2007). *Opt. Lett.*, *32*, 1902.
[14] Byun, K. M., Shuler, M. L., Kim, S. J., Yoon, S. J., & Kim, D. (2008). *J. Lightwave Technol.*, *26*, 1472.
[15] Ruan, L., Yang, F., & Sambles, J. R. (2009). *Appl. Phys. Lett.*, *95*, 171102.
[16] Yang, F., & Sambles, J. R. (1993). *J. Opt. Soc. Am B*, *10*, 858.
[17] Knoesen, A., Moharam, M. G., & Gaylord, T. K. (1985). *Appl. Phys. B*, *38*, 171.
[18] Mbise, G. W., Le Bellac, D., Niklasson, G. A., & Granqvist, C.G. (1997). *J. Phys. D: Appl. Phys.*, *30*, 2103.
[19] Ignatovich, F.V., Ignatovich, V.K. (2012). *Phys. Usp.*, *55*, 709.
[20] Lynch, D.W., & Hunter, W.R. (1985). In: *Handbook of Optical Constants of Solids*, Palik, E.D. (Ed.), Part II, Academic Press: San Diego, 275.
[21] Rakić, A. D., Djurišić, A. B., Elazar, J. M., & Majewski, M. L. (1998). *Appl. Opt.*, *37*, 5271.
[22] Drachev, V. P., Chettiar, U. K., Kildishev, A. V., Yuan, H.-K., Cai, W., & Shalaev, V. M. (2008). *Optics Express*, *16*, 1186.
[23] Kreibig, U., & Vollmer, M. (1985). *Optical properties of metal clusters*, Springer-Verlag: Berlin, Germany.
[24] Kiss, F. D., Miotto, R., & Ferraz, A. C. (2011). *Nanotechnology*, *22*, 275708.
[25] Coronado, E. A., Schatz, G. C. (2003). *J. Chem. Phys.*, *119*, 3926.
[26] Jen, Y. J., & Lee, C. C. (2001). *Opt. Lett.*, *26*, 190.
[27] Smith, G. B. (1990). *Appl. Opt.*, *29*, 3685.
[28] Sihvola, A. (1999). *Electromagnetic mixing formulas and applications*, The Institution of Electrical Engineers: London, UK.
[29] Bohren, C. F., & Huffman, D. R. (1983). *Absorption and Scattering of Light by Small Particles*, John Wiley & Sons: New York.
[30] Born, M., & Wolf, E. (1999). *Principles of Optics*, Cambridge University Press: UK.
[31] Sivuchin, D. (1984). Cours de physique générale: en cinq volumes. *Tome 4, Optique, Éditions MIR*.

[32] Li, J., Wen, C.-H., Gauza, S., Lu, R., & Wu, S.-T. (2005). *J. Disp. Technol.*, *1*, 51.
[33] Liang, Q. T. (1990). *Appl. Opt.*, *29*, 1008.

Appendix

Reflection and transmission coefficients that take into account the phenomenon of nonsymmetrical reflection at the boundaries between the anisotropic and isotropic layers:

$$r_{12} = \frac{\cos\gamma_{12t}(k_{1z+}\varepsilon_{2+} - k_{2z+}\varepsilon_1) - \sin\gamma_{12t}\varepsilon_1\sqrt{k_0^2\varepsilon_{2+} - k_{2z+}^2}}{\cos\gamma_{12t}(k_{2z+}\varepsilon_1 - k_{1z-}\varepsilon_{2+}) + \sin\gamma_{12t}\varepsilon_1\sqrt{k_0^2\varepsilon_{2+} - k_{2z+}^2}},$$

$$t_{12} = \frac{\sqrt{\varepsilon_1\varepsilon_{2+}}(k_{1z+} - k_{1z-})}{\cos\gamma_{12t}(k_{2z+}\varepsilon_1 - k_{1z-}\varepsilon_{2+}) + \sin\gamma_{12t}\varepsilon_1\sqrt{k_0^2\varepsilon_{2+} - k_{2z+}^2}}$$

$$r_{23} = \frac{\sqrt{\varepsilon_{2-}}}{\sqrt{\varepsilon_{2+}}}\frac{\cos\gamma_{23\,i}(k_{3z+}\varepsilon_{2+} - k_{2z+}\varepsilon_3) - \sin\gamma_{23\,i}\varepsilon_3\sqrt{k_0^2\varepsilon_{2+} - k_{2z+}^2}}{\cos\gamma_{23\,r}(k_{2z-}\varepsilon_3 - k_{3z+}\varepsilon_{2-}) + \sin\gamma_{23\,r}\varepsilon_3\sqrt{k_0^2\varepsilon_{2-} - k_{2z-}^2}},$$

$$t_{23} = \frac{\sqrt{\varepsilon_3}}{\sqrt{\varepsilon_{2+}}}\left\{\cos\gamma_{23\,i}\left[\cos\gamma_{23\,r}(k_{2z-}\varepsilon_{2+} - k_{2z+}\varepsilon_{2-}) + \sin\gamma_{23\,r}\varepsilon_{2+}\sqrt{k_0^2\varepsilon_{2-} - k_{2z-}^2}\right]\right.$$
$$\left. - \sin\gamma_{23\,i}\cos\gamma_{23\,r}\varepsilon_{2-}\sqrt{k_0^2\varepsilon_{2+} - k_{2z+}^2}\right\} \Big/$$
$$\left[\cos\gamma_{23\,r}(k_{2z-}\varepsilon_3 - k_{3z+}\varepsilon_{2-}) + \sin\gamma_{23\,r}\varepsilon_3\sqrt{k_{0^2}\varepsilon_{2-} - k_{2z-}^2}\right],$$

$$r_{34} = \frac{\cos\gamma_{34t}(k_{3z+}\varepsilon_{4+} - k_{4z+}\varepsilon_3) - \sin\gamma_{34t}\varepsilon_3\sqrt{k_0^2\varepsilon_{4+} - k_{4z+}^2}}{\cos\gamma_{12t}(k_{4z+}\varepsilon_3 - k_{3z-}\varepsilon_{4+}) + \sin\gamma_{34t}\varepsilon_3\sqrt{k_0^2\varepsilon_{4+} - k_{4z+}^2}},$$

$$t_{34} = \frac{\sqrt{\varepsilon_3\varepsilon_{4+}}(k_{3z+} - k_{3z-})}{\cos\gamma_{12t}(k_{4z+}\varepsilon_3 - k_{3z-}\varepsilon_{4+}) + \sin\gamma_{34t}\varepsilon_3\sqrt{k_0^2\varepsilon_{4+} - k_{4z+}^2}},$$

$$r_{45} = \frac{\sqrt{\varepsilon_{4-}}}{\sqrt{\varepsilon_{4+}}}\frac{\cos\gamma_{45\,i}(k_{5z+}\varepsilon_{4+} - k_{4z+}\varepsilon_5) - \sin\gamma_{45\,i}\varepsilon_5\sqrt{k_0^2\varepsilon_{4+} - k_{4z+}^2}}{\cos\gamma_{45\,r}(k_{4z-}\varepsilon_5 - k_{5z+}\varepsilon_{4-}) + \sin\gamma_{45\,r}\varepsilon_5\sqrt{k_0^2\varepsilon_{4-} - k_{4z-}^2}},$$

$$t_{45} = \frac{\sqrt{\varepsilon_5}}{\sqrt{\varepsilon_{4+}}}\left\{\cos\gamma_{45\,i}\left[\cos\gamma_{45\,r}(k_{4z-}\varepsilon_{4+} - k_{4z+}\varepsilon_{4-}) + \sin\gamma_{45\,r}\varepsilon_{4+}\sqrt{k_0^2\varepsilon_{4-} - k_{4z-}^2}\right]\right.$$
$$\left. - \quad \sin\gamma_{45\,i}\cos\gamma_{45\,r}\varepsilon_{4-}\sqrt{k_0^2\varepsilon_{4+} - k_{4z+}^2}\right\} \Big/$$
$$\left[\cos\gamma_{45\,r}(k_{4z-}\varepsilon_5 - k_{5z+}\varepsilon_{4-}) + \sin\gamma_{45\,r}\varepsilon_5\sqrt{k_0^2\varepsilon_{4-} - k_{4z-}^2}\right],$$

$$r_{21} = \frac{\sqrt{\varepsilon_{2+}}}{\sqrt{\varepsilon_{2-}}}\frac{\cos\gamma_{21i}(k_{1z-}\varepsilon_{2-} - k_{2z-}\varepsilon_1) - \sin\gamma_{21i}\varepsilon_1\sqrt{k_0^2\varepsilon_{2-} - k_{2z-}^2}}{\cos\gamma_{21r}(k_{2z+}\varepsilon_1 - k_{1z-}\varepsilon_{2+}) + \sin\gamma_{21r}\varepsilon_1\sqrt{k_0^2\varepsilon_{2+} - k_{2z+}^2}},$$

$$t_{21} = \frac{\sqrt{\varepsilon_1}}{\sqrt{\varepsilon_{2-}}} \left\{ \cos\gamma_{21\,i} \left[\cos\gamma_{21\,r}(k_{2z+}\varepsilon_{2-} - k_{2z-}\varepsilon_{2+}) + \sin\gamma_{21\,r}\varepsilon_{2-}\sqrt{k_0^2\varepsilon_{2+} - k_{2z+}^2} \right] - \sin\gamma_{21\,i}\cos\gamma_{21\,r}\varepsilon_{2+}\sqrt{k_0^2\varepsilon_{2-} - k_{2z-}^2} \right\} \Big/ \left[\cos\gamma_{21\,r}(k_{2z+}\varepsilon_1 - k_{1z-}\varepsilon_2) + \sin\gamma_{21\,r}\varepsilon_1\sqrt{k_0^2\varepsilon_{2+} - k_{2z+}^2} \right],$$

$$r_{32} = \frac{\cos\gamma_{32t}(k_{3z-}\varepsilon_{2-} - k_{2z-}\varepsilon_3) - \sin\gamma_{32t}\varepsilon_3\sqrt{k_0^2\varepsilon_{2-} - k_{2z-}^2}}{\cos\gamma_{32t}(k_{2z-}\varepsilon_3 - k_{3z+}\varepsilon_{2-}) + \sin\gamma_{32t}\varepsilon_3\sqrt{k_0^2\varepsilon_{2-} - k_{2z-}^2}}$$

$$t_{32} = \frac{\sqrt{\varepsilon_3\varepsilon_{2-}}(k_{3z-} - k_{3z+})}{\cos\gamma_{32t}(k_{2z-}\varepsilon_3 - k_{3z+}\varepsilon_{2-}) + \sin\gamma_{32t}\varepsilon_3\sqrt{k_0^2\varepsilon_{2-} - k_{2z-}^2}}$$

$$r_{43} = \frac{\sqrt{\varepsilon_{4+}}}{\sqrt{\varepsilon_{4-}}} \frac{\cos\gamma_{43i}(k_{3z-}\varepsilon_{4-} - k_{4z-}\varepsilon_3) - \sin\gamma_{43i}\varepsilon_3\sqrt{k_0^2\varepsilon_{4-} - k_{4z-}^2}}{\cos\gamma_{43r}(k_{4z+}\varepsilon_3 - k_{3z-}\varepsilon_{4+}) + \sin\gamma_{43r}\varepsilon_3\sqrt{k_0^2\varepsilon_{4+} - k_{4z+}^2}}$$

$$t_{43} = \frac{\sqrt{\varepsilon_3}}{\sqrt{\varepsilon_{4-}}} \left\{ \cos\gamma_{43\,i} \left[\cos\gamma_{43\,r}(k_{4z+}\varepsilon_{4-} - k_{4z-}\varepsilon_{4+}) + \sin\gamma_{43\,r}\varepsilon_{4-}\sqrt{k_0^2\varepsilon_{4+} - k_{4z+}^2} \right] - \sin\gamma_{43\,i}\cos\gamma_{43\,r}\varepsilon_{4+}\sqrt{k_0^2\varepsilon_{4-} - k_{4z-}^2} \right\} \Big/ \left[\cos\gamma_{43\,r}(k_{4z+}\varepsilon_3 - k_{3z-}\varepsilon_{4+}) + \sin\gamma_{43\,r}\varepsilon_3\sqrt{k_0^2\varepsilon_{4+} - k_{4z+}^2} \right],$$

$$r_{54} = \frac{\cos\gamma_{54t}(k_{5z-}\varepsilon_{4-} - k_{4z-}\varepsilon_5) - \sin\gamma_{54t}\varepsilon_5\sqrt{k_0^2\varepsilon_{4-} - k_{4z-}^2}}{\cos\gamma_{54t}(k_{4z-}\varepsilon_5 - k_{5z+}\varepsilon_{4-}) + \sin\gamma_{54t}\varepsilon_5\sqrt{k_0^2\varepsilon_{4-} - k_{4z-}^2}}$$

$$t_{54} = \frac{\sqrt{\varepsilon_5\varepsilon_{4-}}(k_{5z-} - k_{5z+})}{\cos\gamma_{54t}(k_{4z-}\varepsilon_5 - k_{5z+}\varepsilon_{4-}) + \sin\gamma_{54t}\varepsilon_5\sqrt{k_0^2\varepsilon_{4-} - k_{4z-}^2}}$$

$$\gamma_{21i} = \gamma_{23r}\gamma_{34t} = \gamma_{45i}\gamma_{43i} = \gamma_{45r}\gamma_{mnq}$$

is the angle between the wave vector and ray (Poynting) vector of a chosen wave, determined by expressions $\sin\gamma = \frac{(n_e^2 - n_o^2)\sin\Theta\cos\Theta}{\sqrt{n_e^4\cos^2\Theta + n_o^4\sin^2\Theta}}$ within the anisotropic birefringent LC layer and $\sin\gamma = \frac{\mathrm{Re}(\sqrt{\varepsilon_{z'}} - \sqrt{\varepsilon_{x'}})\sin\Theta\cos\Theta}{\sqrt{(\cos\Theta\mathrm{Re}\sqrt{\varepsilon_{z'}})^2 + (\sin\Theta\mathrm{Re}\sqrt{\varepsilon_{x'}})^2}}$ within the nanorod-array layer (see, e.g., [33]). Θ is the angle between wave vector and optic axis in a uniaxial medium, subscript q in γ_{mnq} refers to the incident (i), reflected (r) or transmitted (t) wave at the interface of the m-th and n-th layers. In these equations $\cos\Theta = \frac{k_x\sin\psi + (\mathrm{Re}k_z)\cos\psi}{\sqrt{k_x^2 + (\mathrm{Re}k_z)^2}}$, $\sin\Theta = \frac{k_x\cos\psi - (\mathrm{Re}k_z)\sin\psi}{\sqrt{k_x^2 + (\mathrm{Re}k_z)^2}}$, $\psi = \varphi$ for the LC layer and $\psi = \beta$ for the nanorod array layer.